

Highly localized clustering states in a granular gas driven by a vibrating wall

Eli Livne¹, Baruch Meerson¹ and Pavel V. Sasorov²

¹ *Racah Institute of Physics, Hebrew University of Jerusalem, Jerusalem 91904, Israel*

² *Institute of Theoretical and Experimental Physics, Moscow 117259, Russia*

An ensemble of inelastically colliding grains driven by a vibrating wall in 2D exhibits density clustering. Working in the limit of nearly elastic collisions and employing granular hydrodynamics, we predict, by a marginal stability analysis, a spontaneous symmetry breaking of the extended clustering state (ECS). 2D steady-state solutions found numerically describe localized clustering states (LCSs). A time-dependent granular hydrodynamic simulation shows that LCSs can develop from natural initial conditions. The predicted instability should be observable in experiment.

PACS numbers: 81.05.Rm, 45.70.Qj, 47.50.+d

Granular flows exhibit fascinating non-equilibrium phenomena and continue to attract much interest [1,2]. We will concentrate here on the striking tendency of granular “gases” (rapid granular flows) to form dense clusters [3]. Clustering results from energy losses by inelastic collisions, and it is a manifestation of thermal condensation instability [4]. Since the discovery of the clustering instability, the validity of granular hydrodynamics [5] has been under scrutiny. In a freely cooling granular gas, all grains eventually come to rest, making the hydrodynamic (and even kinetic) description problematic. In a *driven* granular gas hydrodynamics can be conveniently tested on its steady states. The simplest system of this kind is a submonolayer of grains in 2D, driven by a vibrating side wall at zero gravity. This and related “test bed” systems were investigated by molecular dynamic (MD) simulations [6–8] and in experiment [9]. For sufficiently high average densities, ECS, was observed in these works apart from the driving wall. The basic physics of the ECS is simple. Because of the inelastic collisions the granular temperature decreases with the distance from the driving wall. To maintain the momentum balance, the granular density increases with this distance, reaching the maximum at the opposite (“elastic”) wall. When the density contrast is large enough, the enhanced density region is observed as the ECS.

Comparisons of the steady-state density profiles obtained in MD simulations of this problem with those predicted by granular hydrodynamics showed that hydrodynamics is valid only in the limit of nearly elastic collisions [6–8,10]. This limit has not been fully explored, and it is non-trivial. To show it, we perform a stability analysis of this simple granular system. This analysis reveals a symmetry-breaking instability of the ECS, and formation of LCSs. This result puts this system in the list of pattern-forming systems out of equilibrium [11].

Consider a big ensemble of identical spherical grains of diameter d and mass $m_g = 1$ rolling on a smooth horizontal surface of a rectangular box with dimensions $L_x \times L_y$. The number density of grains is $n(x, y)$. For a submonolayer coverage the maximum value of n corresponds to the

(hexagonal) close-packing value $n_c = 2/(\sqrt{3}d^2)$. Three of the walls are immobile, and grain collisions with them are assumed elastic. The fourth wall (located at $x = L_x$) supplies energy to the granulate. We will consider two different models of energy supply, see below. The energy is being lost through inelastic hard-core grain collisions. We neglect the grain rotation and parameterize the inelasticity of grain collisions by a constant normal restitution coefficient r .

We assume a *strong* inequality $1 - r^2 \ll 1$, which makes a hydrodynamic description valid [6–8]. Therefore, steady states of the system can be described by the equations of momentum and energy balance:

$$p = \text{const}, \quad \nabla \cdot (\kappa \nabla T) = I, \quad (1)$$

where p is the granular pressure, κ is the thermal conductivity, I is the rate of energy losses by collisions and T is the granular temperature. To proceed, one needs an equation of state $p = p(n, T)$ and relations for κ and I in terms of n and T . In the low-density limit, $n \ll n_c$, these relations can be derived from the Boltzmann equation [5]. The high-density limit, $n_c - n \ll n_c$, was considered by Grossman *et al.* [6]. They also suggested convenient interpolations between the low- and high-density limits, and verified them by a detailed comparison with MD simulations. We will adopt this practical approach (see, however, Ref. [12]). In our notation

$$p = nT \frac{n_c + n}{n_c - n}, \quad (2)$$

$\kappa = (\mu/l) n (\alpha l + d)^2 T^{1/2}$ and $I = (\mu/\gamma l) (1 - r^2) n T^{3/2}$. Here l is the mean free path of the grains,

$$l = \frac{1}{\sqrt{8}nd} \frac{n_c - n}{n_c - an}, \quad (3)$$

$a = 1 - (3/8)^{1/2}$, and α and γ are numerical factors of order unity. Grossman *et al.* [6] found that $\alpha \simeq 1.15$ and $\gamma \simeq 2.26$. The value of μ , another numerical factor of order unity, is irrelevant in the steady-state problem.

The boundary conditions include the no-flux conditions $\nabla_n T = 0$ at the “elastic” walls $x = 0, y = 0$

and $y = L_y$. Previously, the “thermal” wall condition $T = \text{const}$ was used at $x = L_x$ [6–8,13]. We will use a different boundary condition, to simulate the vibrating wall more directly. Our main results, however, will be shown to hold for the thermal wall as well.

The problem of computing the energy flux q from a vibrating wall into granulate has been addressed in several works [14]. Let the wall oscillate sinusoidally: $x = L_x + A \cos \omega t$. For small area fractions the granulate near this wall is in the dilute limit. We assume $A \ll l$, so the vibrating wall does not generate any collective motions in the granulate. Grain collisions with the vibrating wall are assumed elastic. Also, ω is much larger than the rate of granular collisions near the vibrating wall, $T^{1/2}/l$, so there are no correlations between two successive grain collisions with the wall. The limit $A\omega \ll T^{1/2}$ was considered by Kumaran [15] for a non-zero gravity. A direct calculation analogous to his, but for zero gravity, yields $q = (2/\pi)^{1/2} A^2 \omega^2 n T^{1/2}$ [16]. In the language of hydrodynamics, q is the heat flux at the wall:

$$\kappa \partial T / \partial x = q \text{ at } x = L_x. \quad (4)$$

Finally, $\int_0^{L_x} \int_0^{L_y} n(x, y) dx dy = \langle n \rangle L_x L_y$ is normalization condition, where $\langle n \rangle$ is the average grain density.

Using Eq. (2), we eliminate T in favor of n and p . In its turn, p can be eliminated by integrating Eq. (1) over the whole box and using the Gauss theorem and Eq. (4). It is convenient to write the governing equations in a scaled form. Introduce scaled coordinates: $\mathbf{r}/L_x \rightarrow \mathbf{r}$ so that the box dimensions become $1 \times \Delta$, where $\Delta = L_y/L_x$ is the aspect ratio of the box. Introducing the (scaled) inverse granular density $z(x, y) = n_c/n(x, y)$, we obtain

$$\nabla \cdot (F(z) \nabla z) = \mathcal{L} Q(z). \quad (5)$$

The boundary conditions are

$$\nabla_n z = 0 \text{ at } x = 0, y = 0 \text{ and } y = \Delta, \quad (6)$$

and

$$\left(G(z) \frac{\partial z}{\partial x} \right) \Big|_{x=1} = \mathcal{L} \frac{\int_0^1 \int_0^\Delta Q dx dy}{\int_0^\Delta H[z(1, y)] dy}. \quad (7)$$

The normalization condition becomes

$$\int_0^1 \int_0^\Delta z^{-1} dx dy = f \Delta, \quad (8)$$

while functions F, G, H and Q are the following:

$$F(z) = \frac{(z^2 + 2z - 1)[\alpha z(z - 1) + \sqrt{32/3}(z - a)]^2}{(z - a)(z - 1)^{1/2} z^{3/2} (z + 1)^{5/2}}, \quad (9)$$

$$G(z) = \frac{(z^2 + 2z - 1)[\alpha z(z - 1) + \sqrt{32/3}(z - a)]^2}{z(z - a)(z - 1)(z + 1)^2}, \quad (10)$$

$$H(z) = \frac{F(z)}{G(z)} \text{ and } Q(z) = \frac{(z - a)(z - 1)^{1/2}}{(z + 1)^{3/2} z^{1/2}}. \quad (11)$$

Finally, $\mathcal{L} = (32/3\gamma) (L_x/d)^2 (1 - r^2)$. The other two governing parameters are the grain area fraction $f = \langle n \rangle / n_c$ and Δ . Notice that the steady-state *density* distributions are independent of A and ω .

Eqs. (5)-(8) make a closed set. Their 1D (y -independent) solution $z = Z(x)$ is described by equations

$$(FZ')' = \mathcal{L}Q, \quad Z'|_{x=0} = 0 \text{ and } \int_0^1 Z^{-1} dx = f, \quad (12)$$

where primes stand for the x -derivatives. Eq. (7) is now satisfied automatically. Eqs. (12) coincide with those obtained by Grossman *et al.* [6] for a *thermal* wall at $x = 1$. Therefore, the *density* profiles of the 1D states coincide for the different types of driving. Eqs. (12) can be solved analytically in the high- and low-density limits [6]. These solutions clearly show that criterion [10] for validity of hydrodynamics is equivalent to a strong inequality $1 - r^2 \ll 1$.

Most interesting among the 1D states is the state with a *dense* cluster (ECS) located at the elastic wall $x = 0$, and a low-density region elsewhere. In this case Eqs. (12) should be solved numerically. Examples are presented in Ref. [6], and a similar clustering state (CS) was observed experimentally [9]. The main objective of this Letter is to show that this state (uniform in the y -direction) can give way, via a spontaneous symmetry breaking, to CSs highly localized in the y -direction. First, a marginal stability (MS) analysis will show, in some region of parameters, loss of stability of the ECS. Then, solving Eqs. (5)-(8) numerically, we will find LCSs. Finally, a time-dependent granular hydrodynamic simulation will show that highly localized CSs can develop from natural initial conditions.

Linearizing Eqs. (5)-(8) around the ECS $z = Z(x)$ and looking for a small correction in the form of $\psi_m(x) \cos(\pi m y / \Delta)$, where $m = 1, 2, \dots$, we obtain

$$F\phi'' - (\mathcal{L}Q_Z + \pi^2 m^2 \Delta^{-2} F)\phi = 0, \quad (13)$$

where $\phi = F\psi_m$ and index Z means the z -derivative evaluated at $z = Z(x)$. The boundary conditions are

$$\phi'|_{x=0} = 0, \quad (FG\phi' + Z'(FG_Z - GF_Z)\phi)|_{x=1} = 0. \quad (14)$$

Functions F and G which enter Eqs. (13) and (14) are evaluated at $z = Z(x)$.

For fixed values of \mathcal{L} , f and m , Eqs. (13) and (14) represent a linear eigenvalue problem for Δ^{-2} , or simply

for the aspect ratio Δ . We denote these eigenvalues by Δ_m , $m = 1, 2, \dots$. Obviously, $\Delta_m(\mathcal{L}, f) = m\Delta_1(\mathcal{L}, f)$. The eigenvalues Δ_m (when they exist) represent the *critical* values of the aspect ratio: at $\Delta > \Delta_m$ the ECS loses stability. For the mode $m = 1$ (or $\lambda/2$, one half of the wavelength across the system in the y -direction) the critical value Δ_1 is the lowest. Figure 1 shows, for different values of \mathcal{L} , the MS curves $\Delta = \Delta_1(f)$ that we found numerically. Above the MS curves LCSs must develop. Interestingly, the ECS remains linearly stable for *any* Δ beyond a finite interval of the area fractions $f_1(\mathcal{L}) < f < f_2(\mathcal{L})$ such that $f_1 > 0$ and $f_2 < 1$. As \mathcal{L} increases, the instability interval (f_1, f_2) shrinks, while the minimum value of Δ_1 decreases: $\Delta_1^{(min)} \simeq 140 \mathcal{L}^{-1/2}$ [17]. For sufficiently large \mathcal{L} , $\Delta_1^{(min)}$ becomes less than 1. See Fig. 2 which shows the instability tongues $m = 1$ and $m = 2$ for $\mathcal{L} = 5 \cdot 10^4$. For higher m we obtain modes $3\lambda/2, 2\lambda, 5\lambda/2, \dots$ which fit in boxes with increasingly larger aspect ratios, $\Delta > m\Delta_1$.

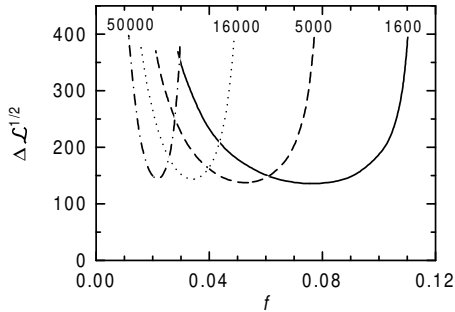


FIG. 1. Marginal stability curves $\Delta_1(f)$ for different values of \mathcal{L} . The values of Δ_1 are multiplied by $\mathcal{L}^{1/2}$.

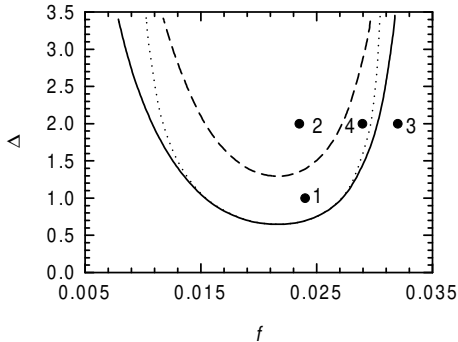


FIG. 2. Marginal stability (MS) curves $\Delta_m(f)$ for $m = 1$ (solid line) and 2 (dashed line) and $\mathcal{L} = 5 \cdot 10^4$. Density profiles corresponding to points 1, 2, 3 and 4 are shown in Fig. 3. The dotted line shows the MS curve $m = 1$ for the “thermal wall”.

When $f \ll \min(1, \mathcal{L}^{-1/2})$, $\Delta_1(f)$ can be found analytically. In this case the whole system is in the dilute limit, $z \gg 1$ (still, it is necessary to account for the sub-leading terms). In addition, $Z(1) - Z(0) \ll Z(0)$ in this case, so Taylor expansion of $Z(x)$ and $\psi(x)$ up to x^4 suf-

fice. After some algebra, Eqs. (12) - (14) yield

$$\Delta_1 = \pi \left(\frac{\mathcal{L}^2 f^4}{3\alpha^4} - \frac{(1+a)\mathcal{L} f^3}{\alpha^2} \right)^{-1/2}. \quad (15)$$

It follows from Eq. (15) that $f_1(\mathcal{L}) = 3\alpha^2(1+a)\mathcal{L}^{-1}$.

The same instability appears when the wall $x = 1$ (in scaled units) is “thermal”. Solving the corresponding eigenvalue problem [where the second boundary condition in Eq. (14) is replaced by $\phi(x = 1) = 0$], we obtained instability tongues similar to those for the vibrating wall, but more narrow. Figure 2 shows the instability tongue $m = 1$ for $\mathcal{L} = 5 \cdot 10^4$. Noticeable is the coincidence of the $m = 1$ curves at intermediate f for the two types of driving. It results from a strong localization of the eigenfunction $\phi(x)$ near the elastic wall $x = 0$ at large \mathcal{L} and intermediate f . The exact form of the boundary condition at $x = 1$ is not important in this regime. Finally, for the thermal wall the LCS is stable for any Δ if $f \ll \min(1, \mathcal{L}^{-1/2})$, in contrast to the vibrating wall.

In the rest of the paper we will deal with the vibrating wall. Within the instability tongues of Fig. 1 the MS analysis is invalid. Besides, it can miss a subcritical bifurcation outside of the instability tongues. Therefore, we solved the 2D steady-state equations (5)-(8) numerically (a nonlinear Poisson solver, Newton’s iterations), exploring some parts of the parameter plane (f, Δ) of Fig. 2. Figure 3 shows the density profiles of 4 typical steady states with $m = 1$ and 2. Highly localized nonlinear $\lambda/2$ - and λ -states are evident in Fig. 3a and b. The maximum/minimum density ratio along the elastic wall $x = 0$ reaches about 21 in these examples.

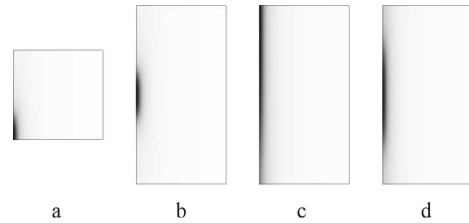


FIG. 3. Steady-state density profiles (gray scale, separate for each picture) corresponding to points 1 (a), 2 (b), 3 (c) and 4 (d) of Fig. 2. The maximum (minimum) density at the wall $x = 0$ is 0.76 (0.036) (a and b), 0.48 (0.21) (c) and 0.54 (0.10) (d). The gas density at the vibrating wall $x = 1$ is close to $4 \cdot 10^{-3}$ for all profiles.

In general, we found that when crossing the MS curve $\Delta = \Delta_1(f)$ from the left (along the line $\Delta = 2$), or from below, one goes continuously from an ECS to a “weakly 2D” $\lambda/2$ -state. This implies a supercritical bifurcation. However, when moving from the right to the left along the line $\Delta = 2$, nonlinear $\lambda/2$ - and λ -states appear *inside* the linear stability regions of the ECS and of the mode $m = 1$, respectively, and *coexist* with the ECS (with the mode $m = 1$, respectively). These findings give evidence

for bistability and subcritical bifurcations. Examples of subcritical $\lambda/2$ - and λ -states are shown in Fig. 3c and d. Super- and subcritical LCSs were also observed for $\Delta = 3$.

A mirror reflection of Fig. 3a with respect to $y = 0$ makes $\Delta = 2$ and produces a λ -state similar to Fig. 2b. Furthermore, extending Fig. 2b periodically in the y -direction, we obtain a periodic chain of LCSs which fit in boxes with increasingly larger aspect ratios. When the aspect ratio goes to infinity, the periodic cluster chain becomes infinite. Cluster chains with *different* periods can fit in boxes with large enough aspect ratios, therefore, an interesting selection problem appears, like in other pattern-forming systems [11].

We performed a series of *time-dependent* hydrodynamic simulations (with $\Delta = 1, 2$ and 3) which showed that the LCSs are dynamically stable and develop from natural initial conditions. We will briefly report here a single simulation with $\Delta = 2$. The full hydrodynamic equations were solved with the same constitutive relations and boundary conditions as in the steady state analysis. Instead of the shear viscosity in the momentum equation we accounted for a small rolling friction force $-n\mathbf{v}/\tau$. An extended version of the compressible hydro code VULCAN [18] was used.

The initial scaled density in this example was $n(x, y, t = 0) = f + 0.1 f \cos(\pi y)$ (independent of x). Figure 4 shows the density evolution. A cluster develops near the elastic wall $x = 0$. With time it becomes localized in the y -direction and approaches the steady-state profile shown in Fig. 3b.

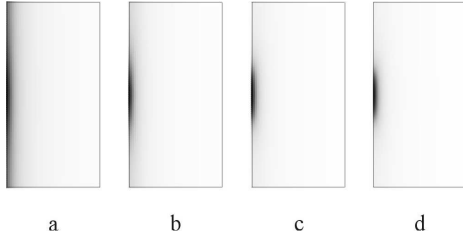


FIG. 4. Density evolution for $\mathcal{L} = 5 \cdot 10^4$, $\Delta = 2$ and $f = 0.0235$. Shown are the density profiles (gray scale, separate for each picture) at scaled times 100 (a), 500 (b), 1,000 (c) and 1,290(d). The maximum (minimum) density at the wall $x = 0$ is 0.25 (0.14) (a), 0.46 (0.072) (b), 0.66 (0.040) (c) and 0.74 (0.036) (d). The gas density at the vibrating wall $x = 1$ is close to $4 \cdot 10^{-3}$ for all profiles.

In summary, we predict a spontaneous transition from an extended to highly localized clustering states in a driven submonolayer granular system. The transition should occur when the aspect ratio is large enough (see Fig. 1). It is insensitive to the vibration frequency and amplitude, and only weakly depends on the type of the driving wall. To observe this transition in experiment, one should minimize the role of the rolling/sliding fric-

tion [9], unaccounted for in our model. The frictional energy losses are proportional to T , while the collisional energy losses are proportional to $T^{3/2}$. Therefore, one should work with higher granular temperatures (that is, larger $A\omega$).

When $1 - r^2$ is *not* small, the normal stress difference, non-Gaussianity in the velocity distribution and possible lack of scale separation become important. The role of these effects in the symmetry-breaking instability should be the subject of further studies.

Finally, the aspect ratios used in Refs. [6,7,9] were always lower than the threshold values for the instability $\Delta_1^{(min)}$. As the result, the instability was suppressed by granular heat conduction in the y direction.

We acknowledge useful discussions with E. Ben-Naim, J. Fineberg and J.P. Gollub. This research was supported by the Israel Science Foundation founded by the Israel Academy of Sciences and Humanities, and by the Russian Foundation for Basic Research (grant No. 99-01-00123).

-
- [1] H.M. Jaeger, S.R. Nagel, and R.P. Behringer, Rev. Mod. Phys. **68**, 1259 (1996); Physics Today, April 1996, p. 32.
 - [2] L.P. Kadanoff, Rev. Mod. Phys. **71**, 435 (1999).
 - [3] M.A. Hopkins and M.Y. Louge, Phys. Fluids A **3**, 47 (1991); I. Goldhirsch and G. Zanetti, Phys. Rev. Lett. **70**, 1619 (1993); S. McNamara and W.R. Young, Phys. Rev. E **53**, 5089 (1996).
 - [4] Similar thermal condensation instabilities develop in radiatively cooling plasmas; for a review see B. Meerson, Rev. Mod. Phys. **68**, 215 (1996).
 - [5] J.T. Jenkins and M.W. Richman, Phys. Fluids **28**, 3485 (1986); C.S. Campbell, Annu. Rev. Fluid Mech. **22**, 57 (1990).
 - [6] E.L. Grossman, T. Zhou, and E. Ben-Naim, Phys. Rev. E **55**, 4200 (1997).
 - [7] J.J. Brey and D. Cubero, Phys. Rev. E **57**, 2019 (1998).
 - [8] S.E. Esipov and T. Pöschel, J. Stat. Phys. **86**, 1385 (1997).
 - [9] A. Kudrolli, W. Wolpert, and J.P. Gollub, Phys. Rev. Lett. **78**, 1383 (1997).
 - [10] Hydrodynamics is expected to be valid when the mean free path of the grains is much smaller than any length scale (and the mean collision time is much smaller than any time scale) described hydrodynamically.
 - [11] M.C. Cross and P.C. Hohenberg, Rev. Mod. Phys. **65**, 851 (1993).
 - [12] Notice that the symmetry-breaking instability predicted in this work does not require very special constitutive relations (CRs). It appears already in the dilute limit described by the “standard” CRs [5].
 - [13] Ref. [7] actually used constant (and equal) temperatures at two opposite walls.
 - [14] S. McNamara and S. Luding, Phys. Rev. E **58**, 813 (1998); and references therein.

- [15] V. Kumaran, Phys. Rev. E **57**, 5660 (1998).
- [16] In the opposite limit $T^{1/2} \ll A\omega$ we found $q = 2\pi A\omega nT$.
An interpolation formula $q = 2\pi A\omega nT (1 + 2^{1/2}\pi^{3/2}\epsilon)^{-1}$
should work well for any $\epsilon = T^{1/2}/(A\omega)$.
- [17] In “physical” units $L_y^{(min)} \simeq 43 \gamma^{1/2} d (1 - r^2)^{-1/2}$.
- [18] E. Livne, Astrophys. J. **412**, 634 (1993).